



# Calculation of the impacts of aerosols on cloud microphysical properties by combining ground- and space-based measurements

Suzanne Crumeyrolle<sup>1</sup>, Quentin Coopman<sup>1</sup>, Eric Bourrienne<sup>1</sup>, Clara Lapointe<sup>1</sup>, Eloise Delbarre<sup>1</sup>, Elise  
5 Devigne<sup>1</sup>, Olivier Pujol<sup>1,2</sup>, Romain De Filippi<sup>1</sup>, Timothy J. Garrett<sup>3</sup>

<sup>1</sup> Univ. Lille, CNRS, UMR 8518 – LOA – Laboratoire d’Optique Atmosphérique, F-59000 Lille, France

<sup>2</sup> Institut Universitaire de France (IUF)

<sup>3</sup> Department of Atmospheric Sciences, University of Utah, 135 S 1460 E Rm 819, Salt Lake City, UT 84112, USA;

10

*Correspondence to:* Suzanne Crumeyrolle (suzanne.crumeyrolle@univ-lille.fr)

## Abstract.

The effect of aerosols on cloud properties remains poorly constrained, in part because ground-based measurements are highly local while space-based retrievals are spatially imprecise. Here, we show how the two viewpoints can be combined using  
15 colocated surface aerosol measurements and thermodynamic profiling from the peri-urban ATOLL (ATmospheric Observatory in LiLLe) site and geostationary-satellite cloud microphysical retrievals from the SEVIRI instrument. Focusing on low-level stratiform clouds that formed under thermodynamically stable conditions, we relate cloud properties to aerosol light scattering as a proxy for cloud condensation nucleus concentrations for two cloud liquid water path bins of 20-100 and 100–200 g m<sup>-2</sup>. Relative changes of cloud droplet number concentrations and effective radii are compared to relative changes  
20 in aerosol light scattering coefficient to find respective susceptibilities. The susceptibility of the cloud droplet number concentration to the aerosol scattering coefficient ( $S_n$ ), also called nucleation efficiency, is retrieved around 0.29 for LWP (Liquid Water Path, from 20 to 100 g m<sup>-2</sup>) and around 0.30 for higher LWP (between 100 to 200 g m<sup>-2</sup>). For the same LWP ranges, the susceptibility of the effective radius to the aerosol burden ( $S_{re}$ ) is around 0.08 and 0.07, respectively. These values are consistent with, although on the lower side of, prior studies of continental stratus. Uncertainties in this study are dominated  
25 by a small sample size and satellite retrieval biases. However, the approach is readily extensible to other ground-based sites measuring boundary layer aerosol concentrations pointing towards a method for better constraining susceptibility calculations globally.



## 30 1 Introduction

That the radiative properties of clouds respond to aerosols is no longer in question (Boucher et al., 2013). The magnitude of aerosol-cloud interactions (ACI), however, remains among the largest sources of uncertainty in Earth’s radiative budget (Quaas et al., 2010, Bellouin et al., 2020; Watson-Parris and Smith, 2022; Michibata, 2022; Duran et al., 2025) due to the complexity of atmospheric processes as well as observational limitations (Fan et al., 2016). Current assessments suggest uncertainties of  
35 more than  $\pm 1 \text{ W m}^{-2}$ , comparable in magnitude to the estimated forcing itself (Bellouin et al., 2020; Forster et al., 2021).

Ground, satellite, and in-situ measurements have been used to estimate the susceptibility of cloud properties to aerosol burden. Satellite measurements of those susceptibilities have the advantage of being nearly global in scope, as well as observing the tops of clouds—the part that most directly reflects incoming solar radiation and is therefore most relevant to Earth’s energy budget. However, such studies can be limited by how cloud moisture and reflected radiation contaminate retrievals of adjoining  
40 aerosol fields, as well as by the range of assumptions embedded in the retrieval algorithms of cloud liquid water path, droplet number concentration and diameter (Grosvenor et al., 2018; Jia et al., 2021). Because clouds are bright, it is not possible to simultaneously observe from space aerosol properties directly below them, which is where they are most relevant (Gryspeerd et al., 2016; Jia et al., 2021). Moreover, even in adjacent air, retrievals of aerosol optical depth (AOD) or aerosol index (AI) lack vertical resolution, and so they may include aerosols located at heights different from those that directly impact the  
45 observed clouds, e.g. the free troposphere rather than the boundary layer (Quaas et al., 2020).

Quaas et al. (2020) argue that in situ and ground-based measurements are better suited for quantifying relevant processes that remain poorly constrained by satellite observations, particularly finer scale processes such as air parcel updraft variability and aerosol spatial inhomogeneity. Airborne studies can capture cloud details, but are unsuitable for long term monitoring. Ground-based measurements can excel at measuring changes in aerosol concentration and chemistry, as well as boundary layer  
50 thermodynamic structure (Rosenfeld et al., 2014; Sena et al., 2016), but only few long-term ground-based sites exist that are capable of monitoring both aerosols and clouds. Even then, their insights are necessarily local, with uncertain global generality (McComiskey et al., 2009; Sarna & Russchenberg, 2016). Similarly, ground-based stations may measure a wide range of radiatively relevant cloud parameters using remote sensing instruments (McComiskey et al., 2009; Madhavan et al., 2012; Kim et al., 2012; Garrett & Zhao, 2013; Sarna & Russchenberg, 2016; Sena et al., 2016; Qiu et al., 2017; Zheng et al., 2020), but  
55 they are inherently limited by their temporal and geographical location.

We propose here that combining space- and ground-based perspectives may offer an alternative path forward. We show how cloud droplet concentration and radius susceptibilities to aerosol burden can be calculated by taking advantage of the “best of both worlds”, using in-situ aerosol observations obtained from a ground station and cloud properties retrieved from space (Lihavainen et al., 2010, Nandan et al., 2022). We harness the temporal resolution of geostationary satellites that are monitoring  
60 the radiative properties of clouds and compare them with surface-based aerosol measurements directly below—linking them



in both space and time. For these susceptibility estimates, our study focuses on low-level stratiform clouds formed under thermodynamically stable conditions using ground-based aerosol data obtained in the North of France and SEVIRI satellite imagery. This work should be viewed as a proof-of-concept study. By applying the methodology to a single, well-characterized site, we explore its strengths, limitations, and underlying assumptions. The broader objective is to lay the groundwork for future applications across a network of sites, rather than to draw generalized conclusions from the present analysis.

## 2 Materials

### 2.1 Ground based Measurements

The ATOLL observatory (50.6114° N, 3.1406° E; 60 m a.s.l.), shown in Figure 1, operates within the ACTRIS framework (Pandolfi et al., 2021) and is located in Villeneuve d'Ascq, a suburban area situated a few kilometers from the city of Lille, the central core of a densely populated metropolitan region. The surrounding environment is characterized by a mix of emission sources including traffic, residential heating, agricultural practices, industrial activities, and contributions from maritime transport (Chen et al., 2022). Measurements reported at this site (Velazquez-Garcia et al., 2023) highlight aerosol properties consistent with those typically observed in urban conditions, as defined within the GAW classification scheme (Laj et al., 2020; Rose et al., 2021). In addition to local influences, the site occasionally experiences the impact of air masses transported over long distances, bringing in particles associated with volcanic activity or Saharan dust events (Mortier et al., 2013; Bovchaliuk et al., 2016; Boichu et al., 2019).

#### 2.1.1 In situ measurements

The analysis presented here relies on observations collected between 2020 and 2024. Aerosol sampling was conducted through individual stainless-steel lines, each positioned at least one meter above the rooftop to limit microscale interferences. Depending on the instrument, the inlets were fitted with either PM<sub>1</sub> or PM<sub>10</sub> size-selective devices. Downstream the inlets, nafion membranes are operated to keep relative humidity below 40%, following ACTRIS guidelines.

Particle number size distributions spanning diameters from 10 to 800 nm were obtained with a time resolution of 5 minutes using a Scanning Mobility Particle Sizer (SMPS). The system combined a differential mobility analyzer (DMA, TSI 3082; Villani et al., 2007), a Ni-63 neutralizer (95 MBq), and a condensation particle counter, initially a TSI 3775 and later replaced by a TSI 3750 (from May 2022). Instrumental configuration evolved slightly over time, notably with a reduction of the lower detectable particle diameter from 15.7 nm to 10 nm starting in May 2022. Airflow conditions within the SMPS were maintained via a closed-loop arrangement regulated by a critical orifice (Jokinen and Mäkelä, 1997). Each measurement cycle lasted 300 seconds. Corrections applied during data processing included adjustments for particle charging probabilities and diffusional losses, implemented with the AIM software (version 10.2.0.11). To ensure robustness, integrated particle concentrations



90 derived from the SMPS were regularly checked against an independent condensation particle counter (TSI 3775 and later TSI 3750).

Aerosol optical properties were derived from measurements of total and backscattering coefficients under dry conditions. For this purpose, two nephelometers (Aurora 4000 and Aurora 3000, Ecotech) operating at 450, 525, and 635 nm were deployed (Müller et al., 2009, 2011). The configuration allowed sequential characterisation of coarse and fine fractions, with the Aurora 95 4000 sampling PM<sub>10</sub> particles and the Aurora 3000, located downstream of a PM<sub>1</sub> cyclone, targeting the finer fraction. Only the PM<sub>10</sub> dataset is considered in the present work. Instrument performances were monitored through daily zero measurements carried out with particle-free air to account for variability in gas-phase scattering contributions, such as those related to nitrogen dioxide. Calibration procedures were conducted periodically using carbon dioxide. Finally, the raw scattering data were corrected to account for known instrumental limitations, including angular truncation and non-ideal illumination, following 100 the approach described by Müller et al. (2009).

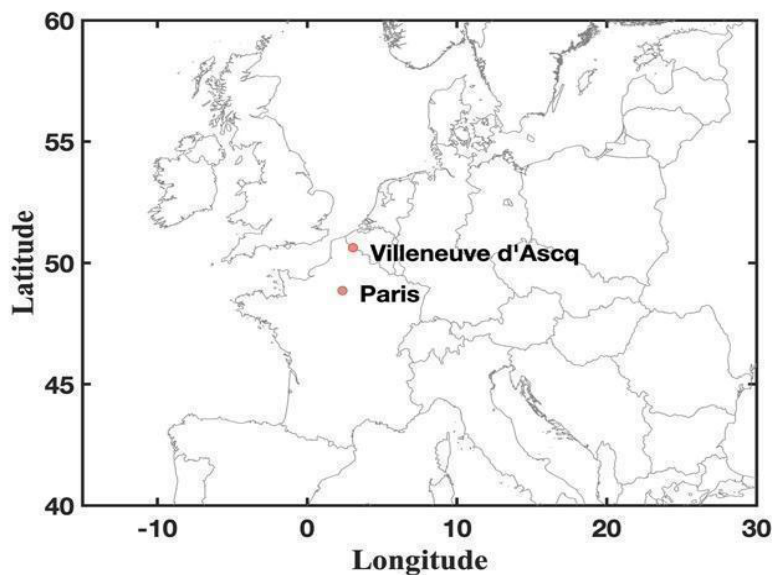


Figure 1: Geographic location of the ATOLL station in Villeneuve d'Ascq (northern France).

### 2.1.2 Boundary layer profiling

The microwave profiler RPG-HATPRO G5 (MWRP G5) measures the radiation in the 20-29 GHz and 50-59 GHz ranges emitted by the troposphere. Using a neural network adapted to the radiometer geographic situation and trained by around 25000 105 profiles, the MWRP G5 provides retrievals of tropospheric vertical profiles (0 – 10 km) of absolute humidity and temperature.



From these data, relative humidity profiles can be calculated, as well as other thermodynamic quantities (eg. potential temperature, liquid water content, etc). The vertical resolution is around 30 m in the boundary layer (BL) and decreases for higher altitudes (around 100 m from the BL up to 5 km and 400 m from 5 to 10 km). The MWRP allows for the monitoring of the thermodynamic state of the atmosphere with its high temporal resolution (1 min). The profile accuracies are around 0.6 K  
110 RMS (Root Mean Square, for temperature profiling) and 0.4 g m<sup>-3</sup> RMS. A wide variety of weather phenomena where water vapour plays an important role can therefore be measured (e.g., Louf et al, 2015; Mascout et al. 2023a, b, 2022; Miri et al. 2024). The MWRP is also equipped with in situ sensors for ground level measurement of temperature, water vapour, pressure, wind direction and velocity.

115

Boundary-layer height (BLH) is retrieved from the microwave-radiometer thermodynamic profiles using the virtual potential temperature ( $\theta_v$ ), see Equation 1 and Equation 2. BLH is defined as the altitude of the minimum of  $\partial\theta_v/\partial z$  above the surface within the lowest few kilometers. If  $\partial\theta_v/\partial z$  has no minimum, then BLH is automatically set to zero. Similar methods have been applied to MWRP temperature profiles by Sinclair et al. (2022), Moreira et al. (2020) and Collaud Coen et al. (2014) to  
120 diagnose the BLH.

$$\theta_v = \theta(1 + 0.61q_v) \quad (1)$$

$$\theta = T \left( \frac{p_0}{p} \right)^{\frac{R}{C_p}} \quad (2)$$

Where  $T$  is air temperature (K),  $p$  pressure (Pa),  $p_0$  (equal to 1000 hPa) a reference pressure,  $q_v$  the specific humidity (kg kg<sup>-1</sup>),  $R$  the gas constant for dry air (i.e. 287.05 J K<sup>-1</sup> kg<sup>-1</sup>), and  $C_p$  the specific thermal capacity of dry air at constant pressure (i.e. 1004 J K<sup>-1</sup> kg<sup>-1</sup>).  
125

The MWRP is also able to provide vertical profiles of the liquid water content (LWC) derived from the adiabatic limit using the empirical relation of Karstens et al. (1994). By vertical integration, the liquid water path is estimated.  
130

## 2.2 Space-based cloud properties CLAAS-3

Satellite observations are used to retrieve optical and microphysical properties of clouds. On the one hand, instruments on polar orbiting satellites have a better spatial resolution, e.g., about 1 km spatial resolution for cloud products from MODIS  
135 instruments for example (Platnick et al., 2003), covering the Earth surface in one day, so that only one measurement per day can be co-located with ground-based observations. On the other hand, instruments on geostationary satellites have a lower



spatial resolution, but observe Earth from the same perspective, and the retrievals are therefore more suitable for co-location with ground-based observations. The Spinning Enhanced Visible and Infrared Imager (SEVIRI), on board the geostationary METEOSAT second generation satellites, has a temporal resolution of 15 minutes and measures in four visible and near-  
140 infrared channels and eight infrared channels with a spatial resolution of 3 km and 1 km respectively (Schmetz et al., 2002) at the sub-satellite point ( $0^\circ$  longitude and latitude). At the latitude and longitude of the ATOLL station, the spatial resolution of SEVIRI is about  $5 \times 5$  km<sup>2</sup>.

The CCloud property dAtAset using SEVIRI - edition 3 (CLAAS-3, Benas et al., 2023) retrieves cloud properties based on  
145 measurements in the visible and near infrared. Cloud detection is performed using a naive Bayesian approximation. Cloud observations from the space-based Lidar CALIOP and SEVIRI reflectances were used to train the algorithm. Cloud top pressure is retrieved from a multilayer perceptron neural network trained with data from CALIOP and SEVIRI measurements in the infrared channels (3.7, 8.5, 11, and 12  $\mu\text{m}$ ). Cloud thermodynamic phase is inferred from an adapted algorithm described by Pavolonis et al. (2005) based on a decision tree measurement from infrared channels (3.9, 6.3, 8.7, 10.8, 12, and 13.4  $\mu\text{m}$ ).  
150 The algorithm retrieves six different types of clouds: liquid, supercooled, opaque ice, cirrus, overlap and overshooting. Only liquid clouds are studied here, so only the first two categories are considered. Cloud optical thickness ( $\tau$ ) and cloud droplet effective radius ( $r_e$ ) are determined using a look-up table following the method of Nakajima and King (1990) via a visible channel at 0.6  $\mu\text{m}$  and a shortwave infrared channel at 3.9  $\mu\text{m}$ . The liquid water path (LWP) is retrieved from the cloud optical depth and  $r_e$  assuming a vertically homogeneous water content, following the method from Stephens (1978). Cloud droplet  
155 number concentration ( $n_d$ ) is also retrieved from the cloud optical depth,  $r_e$  considering an idealized stratiform boundary layer cloud with a fixed dispersion of the assumed cloud droplet size distribution (Bennartz & Rausch, 2023).

A comprehensive evaluation of CLAAS-3 is given in Benas et al. (2023). A comparison of the cloud thermodynamic phase with CALIPSO shows that the liquid cloud fraction can differ by up to 30% in some regions and is less than 10% above the  
160 ATOLL station. The difference is even smaller if upper clouds with  $\tau$  less than 0.1 are excluded from CALIOP measurements. Cloud optical depth,  $r_e$ , LWP and  $n_d$  were compared with AMSR2, MODIS, and in situ measurements. A correlation coefficient of 0.79 was retrieved between the liquid water path from CLAAS-3 and from AMSR-2 measurements. Coefficients of determination of 0.53 and 0.58 have been retrieved between  $\tau$  and  $r_e$  respectively from CLAAS-3 using the 3.9  $\mu\text{m}$  channel and from MODIS measurements using 3.7  $\mu\text{m}$  (Benas et al., 2023). Similarly, a correlation coefficient of 0.71 was retrieved  
165 between  $n_d$  from CLAAS-3 and MODIS measurements. Lastly, it is important to acknowledge that several biases in the measurements could introduce uncertainties. These include (CMSAF, 2022): (i) the assumption of plane-parallel clouds, (ii) passive satellite sensors measuring an averaged radiance of both cloudy and cloud-free areas within a pixel, (iii) surface brightness, (iv) the measured signal originating from an integrated profile, (v) LWP retrievals assuming a vertically uniform  $r_e$ , while  $n_d$  retrievals assume an increasing  $r_e$  with height, which is more representative of stratocumulus clouds, (vi) aerosols  
170 above clouds not being considered in the retrievals, and (vii)  $r_e$  and  $\tau$  being retrieved from look-up tables using the doubling



adding Koninklijk Nederlands Meteorologisch Instituut (KNMI) method (Wolters et al., 2006), assuming liquid clouds between 1 and 2 km in height.

**Table 1: Cloud and Aerosol Properties Measured or Derived from Observations at ATOLL, France.**

Measured parameter	Acronym (SI unit)	Instrument and algorithm	Citation
Cloud droplet number concentration	$n_d$ (cm <sup>-3</sup> )	SEVIRI/CLAAS3	Benas et al. (2023); Bennartz & Rausch, 2017
Cloud droplet effective radius	$r_e$ (μm)	SEVIRI/CLAAS3	Benas et al. (2023); Nakajima and King (1990)
Total aerosol light scattering coefficient	$\sigma_{sp}$ (Mm <sup>-1</sup> )	AURORA 4000	Müller et al. (2009, 2011)
Condensation nuclei	CN (cm <sup>-3</sup> )	SMPS	Villani et al. (2007)
Temperature and relative humidity profiles	T (K) and RH (%)	MWRP	Cimini, et al. (2004)
Boundary layer height	BLH (km)	MWRP	Sinclair, et al. (2022)
Cloud liquid water path	LWP (g m <sup>-2</sup> )	MWRP	Stephens (1978)
Cloud top and cloud base	CT and CB (km)	MWRP	Mascaut et al. (2022, 2023a, b)

### 175 3 Methodology

In this study, we leverage a comprehensive dataset combining in-situ and remote sensing observations from both ground-based and satellite platforms to investigate aerosol-cloud interactions (see section 4) over the 2020–2024 period. The objective is to relate aerosol properties measured near the surface to cloud microphysical properties observed from space, necessarily requiring a set of physical and observational assumptions. Ground-based datasets are point measurements, whereas space-based measurements on a pixel-by-pixel basis cover a larger area. However, all ground-based datasets were temporally resampled to match the measurement frequency of the CLAAS-3 retrievals (0.0011 Hz, corresponding to 15-minute intervals). As shown by Velazquez Garcia et al. (2023) over a three-year period (2016–2019), the mean wind speed over ATOLL was approximately 3 m s<sup>-1</sup> and only rarely exceeded 5 m s<sup>-1</sup>. Thus, the temporal sampling interval corresponds with an advection distance at the ground that is closely consistent with satellite-derived cloud properties averaged over a larger spatial footprint (up to 4.5 km).



The following sections describe the criteria used to filter and classify the dataset in order to identify conditions suitable for calculating the cloud property susceptibility to aerosol burden using combined ground and space-based measurements of aerosols and clouds. Specifically, we select cases: (i) where the observed cloud base height is within the BL, suggesting a direct coupling between surface aerosols and clouds (Section 3.1), (ii) where the lower atmosphere is thermodynamically stable, favouring persistent low-level clouds and reducing dynamic variability (Section 3.2) and (iii) where the relative error of LWP measured by both the radiometer and satellite is below 60% indicating that the scenes observed by both platforms are similar (Section 3.3) and (iv) where aerosol scattering exhibits a strong correlation with proxies for cloud condensation nuclei (CCN) (Section 3.4).

### 195 **3.1 Low altitude cloud criteria**

Our analysis focuses exclusively on aerosol measurements within the BLH, and we restrict our analysis to cases where the clouds are embedded within it. To identify such conditions, we use ground-based MWRP observations to determine the height of the boundary layer height (e.g., Sinclair et al., 2022). Cloud base and top heights are inferred from MWRP-derived LWC profiles, with a threshold of  $0.01 \text{ g m}^{-3}$  for cloud detection. To retain only stratiform BL clouds, we only consider clouds with a LWP  $< 200 \text{ g m}^{-2}$  (Pruppacher and Klett., 2010), with a cloud base lying beneath the estimated BL height but above 100 m to exclude fog and raining events. This filtering ensures that we consider only low-level clouds that are mixed with BL aerosols, thereby minimising uncertainties related to decoupled layers or complex thermodynamic structures. Applying this criterion reduces the dataset to 18% of the original dataset consisting of valid data in which all instruments (SMPS, Nephelometer, MWRP and SEVIRI) simultaneously provide valid data.

205

### **3.2 Atmospheric stability criteria**

Atmospheric dynamics play a critical role in cloud formation and evolution (Klein & Hartmann, 1993). To isolate the influence of aerosols on cloud microphysics, we restrict our analysis to meteorologically stable conditions (Coopman et al., 2018). Atmospheric stability was assessed using temperature and humidity profiles derived from ground-based MWRP observations, combined with surface measurements to compute the equivalent potential temperature ( $\theta_e$ ) at both the surface and the top of the cloud layer. The vertical gradient of  $\theta_e$  — calculated as the difference between these two levels — served as an indicator of moist stability. Only cases with positive gradients, indicative of thermodynamically stable stratification with respect to a moist adiabatic, were retained for further analysis. Additionally, to ensure that only stratiform clouds were included, we excluded all clouds with a geometric thickness greater than 1 km, effectively filtering out cumulus clouds. This approach minimises the influence of convective mixing and dynamic lifting on cloud development. Moreover, we only kept cases when the BLH was larger than 500m. Applying these stability and cloud-type criteria reduced the dataset to approximately 40% of its original size.

215



### 3.3 Similar scenes

220 In order to retrieve accurately low cloud microphysical properties, including  $n_d$  and  $r_e$  from satellite observations, one needs to ensure that both scenes observed by ground based and satellite platforms are similar and therefore removing cases when there are overlying cloud layers. To do so, ground-based LWP measurements from the MWRP were compared with satellite-retrieved LWP from CLAAS-3. Only observations with relative differences not exceeding 60% were retained to ensure comparability. Applying this criterion reduces the dataset to 45% of the original sample.

### 3.4 Cloud condensation nuclei criteria

225 Aerosol properties measured at the surface are used as a proxy for the aerosol population interacting with the cloud base. This assumption is made for practical reasons, as direct observations at cloud base are not available. However, since cloud susceptibilities to aerosol burden is quantified in terms of relative changes, the metric is relatively insensitive to absolute differences in aerosol concentration: changes in surface aerosol concentrations are assumed to scale proportionately with changes at cloud base.

230 CCN are not directly measured at ATOLL. Fine aerosols (with diameters  $D_p$  less than 100 nm) are generally inefficient both in acting as CCN and in scattering light (Dusek et al., 2006). Figure 2 compares the aerosol number concentration (CN) and  $\sigma_{sp}$  data between 2020 and 2024 when the dataset is constrained or not for CCN. The highest aerosol concentrations were typically observed during the summer months, coinciding with the peak frequency of new particle formation events (Crumeyroille et al., 2023). During these periods, CN concentrations often reached values larger than  $10\,000\text{ cm}^{-3}$ . A threshold for the effective radius (greater than 39 nm) calculated from the SMPS size distribution measurements was used to remove cases when aerosols are too small to serve as CCN (Garrett et al., 2004). Using this threshold allows the maximisation of the correlation coefficient (from 0.13 to 0.34) between CN and  $\sigma_{sp}$  and the retention of 20% of the initial database (Table 2).

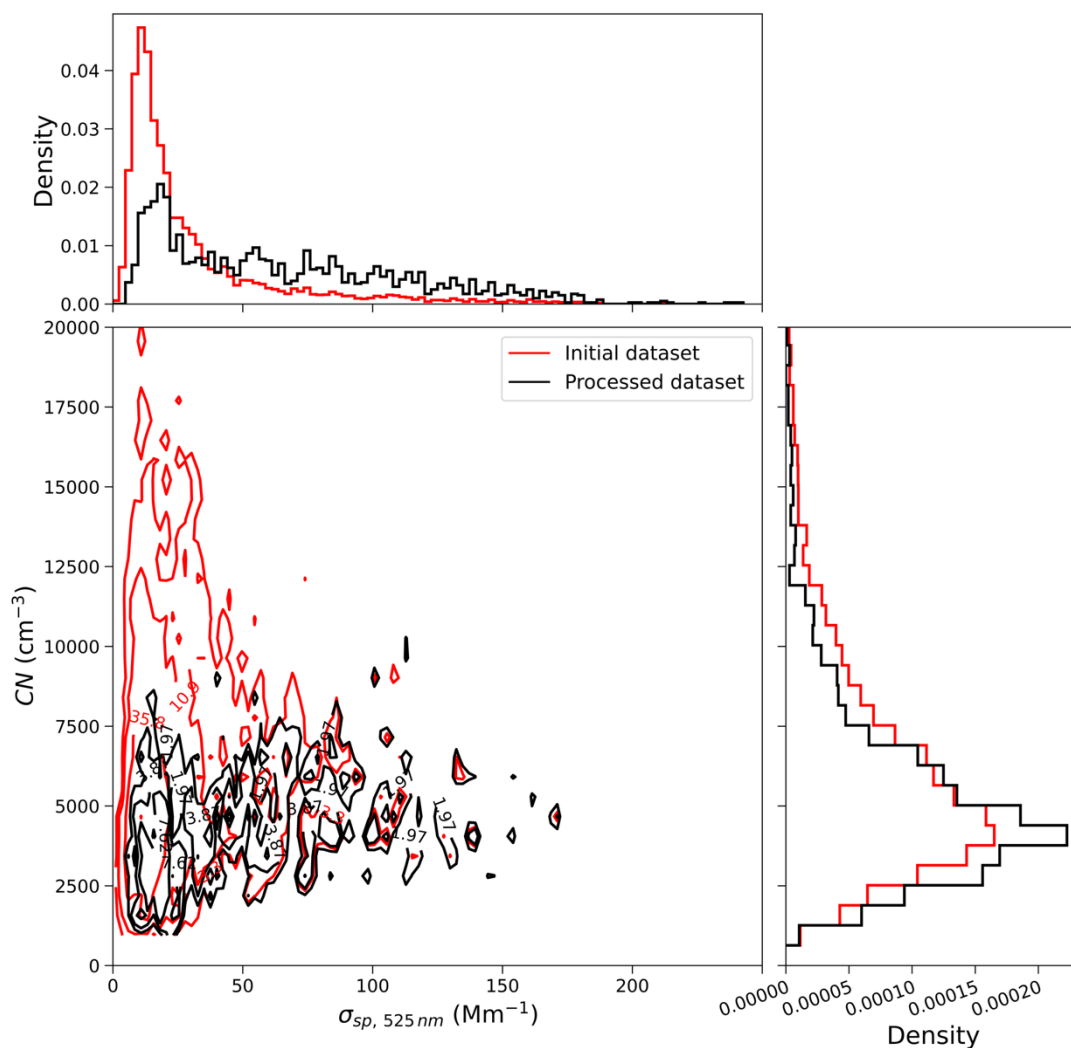


**Figure 2:** A 2-D histogram of the aerosol number concentrations (CN) and dried aerosol light scattering ( $\sigma_{sp,525nm}$ ) measured at ATOLL from 2020 to 2024 when the dataset is not constrained (in red) and when the CCN criteria is applied (in black) following Garrett et al. (2004). The histograms on the right and on the top are the normalized histograms of CN and  $\sigma_{sp,525nm}$  respectively when the dataset is not constrained (in red) and when the CCN criteria is applied (in black).



240 **Table 2: Number of valid data points retained for the study. Initial database corresponds to cases when CLAAS3 and ground based in situ/remote sensing instruments are simultaneously available (8389). The low altitude cloud, atmospheric stability, similar scenes and CCN criteria were then applied individually and simultaneously (All combined) to the initial database.**

	Initial database	Low altitude cloud	Atmospheric Stability	Similar scenes	CCN	All combined
Number	8389	1534	3314	3754	1648	188
percentage	100%	18%	40%	45%	20%	2%

When applied individually to the dataset, low cloud altitude, atmospheric stability, similar scenes and the CCN criteria retained 18%, 40%, 45% and 20% of the total cases, respectively (see Table 2). However, when applied simultaneously, only 2% of the original dataset (188 out of 8389 cases) remained. Assuming the four criteria were statistically independent, we would expect less than 1% of the dataset to satisfy all four criteria simultaneously. The much larger observed overlap (2%) indicates that those criteria are not fully independent and may overlap less than expected, meaning some cases simultaneously satisfy multiple conditions more often than random chance would predict. While this stringent filtering significantly reduces the sample size, it improves the physical consistency of the selected cases and ensures that retained cases are representative of the targeted regime. These selected data points represent situations with minimal uncertainty in cloud-aerosol attribution and meet all requirements in terms of temporal and spatial collocation, cloud type, aerosols and boundary layer conditions. Therefore, despite their limited number, these cases provide a robust and representative basis for our analysis.

Figure 3 presents a climatology of  $r_e$ ,  $n_d$ , CN,  $\sigma_{sp,525nm}$ , and  $d\theta/dz$ , alongside the number of data points retained after applying the constraints. Following the filtering process, 30% of all data points are observed during winter, while only 15% are observed during summer. This disparity primarily stems from the stability filter: since  $d\theta/dz$  is typically higher in winter, more data points meet the criteria during this season. For the cloud parameters, no distinct seasonal trends emerge; instead, they exhibit relative constancy throughout the year. Indeed,  $r_e$  and  $n_d$  unconstrained climatologies (Figure S1) are similar to the constrained ones (Figure 3).



260

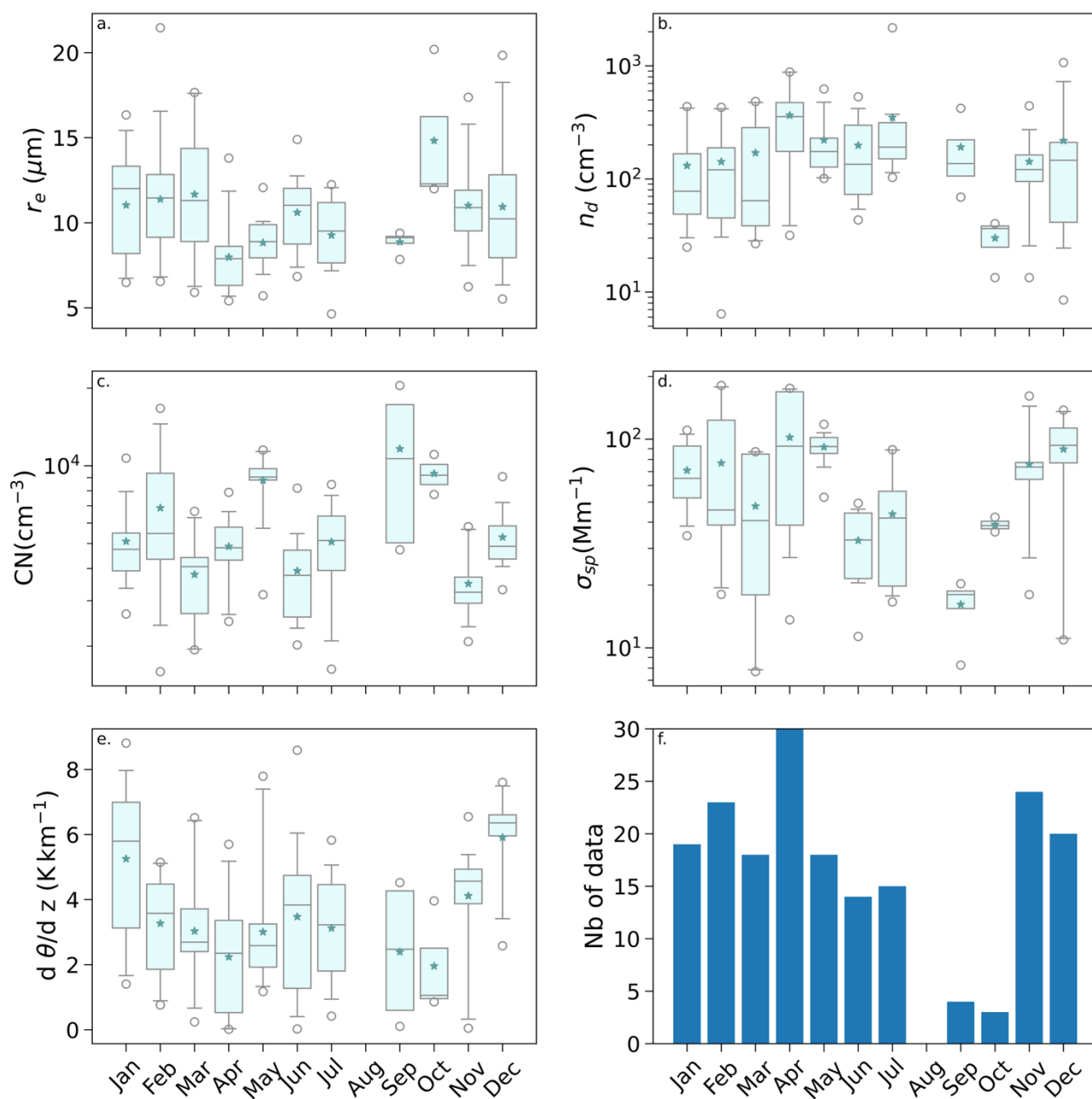


Figure 3: Climatologies of (a) cloud droplet effective radius ( $r_e$ ), (b) cloud droplet number concentration ( $n_d$ ), (c) particle concentration (CN), (d) dried aerosol light scattering ( $\sigma_{sp,525nm}$ ), (e) potential temperature vertical gradient ( $d\theta/dz$ ), and (f) the number of observations (Nb of data) over the ATOLL station when all filters described in section 3 are applied. For subfigures a to

265



e, the box represents the interquartile range (25th–75th percentiles), with the median indicated by a horizontal line and the mean by the star. Whiskers extend to the 1st and 99th percentiles and outliers of the whiskers are shown as individual points.

## 4 Preliminary results & Discussion

### 4.1 Cloud droplet number concentration

270 The relationships between the  $n_d$  and  $r_e$  and the aerosol scattering coefficient ( $\sigma_{sp,525nm}$ ) are illustrated in Figures 4 and 5, respectively, for two ranges of LWP derived from the MWRP observations: from 20 to 100 g m<sup>-2</sup> and from 100 to 200 g m<sup>-2</sup>. We observe that  $n_d$  increases with  $\sigma_{sp,525nm}$  for both LWP ranges. For low LWP,  $n_d$  values rise from 69 cm<sup>-3</sup> at a scattering coefficient around 8.0 Mm<sup>-1</sup> to 170 cm<sup>-3</sup> around 180 Mm<sup>-1</sup>. For larger LWP values,  $n_d$  values rise from 96 cm<sup>-3</sup> at a scattering coefficient around 8 Mm<sup>-1</sup> to 243 cm<sup>-3</sup> at 170.0 Mm<sup>-1</sup>. This observation aligns with previous studies that have explored the

275 relationship between aerosol scattering properties and droplet formation. For example, Garrett et al. (2004) demonstrated that higher scattering coefficients are often associated with increased aerosol concentrations, which can act as CCN, thereby facilitating the formation of a greater number of droplets. Similarly, MacDonald (2020) and Motos et al. (2023) reported that enhanced scattering is indicative of larger particle sizes or higher particle number concentrations, both of which contribute to increased droplet nucleation rates.

280

The cloud droplet concentration susceptibility to aerosol scattering coefficient, or nucleation efficiency ( $S_n$ ), is defined as:

$$S_n = \frac{d \ln(n_d)}{d \ln(\sigma_{sp})} \quad (3)$$

285 To assess the uncertainty associated with the linear regression slope in log-log space, we calculated the standard error of the slope based on the residual variance and the spread of the independent variable, and derived a 95% confidence interval. This interval provides a statistically robust range within which the true slope is expected to lie, thus offering a quantitative estimate of regression uncertainty. Over the period of interest, we find that the cloud droplet concentration susceptibility ( $S_n$ ) is ranging from  $0.29 \pm 0.27$  for low liquid water paths ( $20 < \text{LWP} < 100 \text{ g m}^{-2}$ ) to  $0.30 \pm 0.25$  for thicker clouds ( $100 < \text{LWP} < 200 \text{ g m}^{-2}$ ). Often, observations above 150 g m<sup>-2</sup> are excluded from consideration to avoid precipitating clouds (McComiskey et al.,

290 2009). As these cases do not impose any constraint on the fit, either upward or downward, we choose to keep such cases due to the low number of data points but those observations are highlighted (red circles) in Figures 4 and 5. Generally, as expected, an increased aerosol loading leads to higher cloud droplet concentrations.

These results are comparable in magnitude, though somewhat lower, than those reported in the literature. Quaas et al. (2009),

295 based on satellite retrievals and model simulations, reported  $S_n$  values ranging from 0.07 to 0.64 over land, and from 0.11 to 0.78 over ocean, though the LWP range considered was not specified. Sarna and Russchenberg (2016), using ground-based



remote sensing retrievals of droplet number concentration and integrated attenuated backscatter, found  $S_n$  values between 0.78 and 1.59 for two case studies with LWP between 30 and 90  $\text{g m}^{-2}$ . In a larger statistical analysis, McComiskey et al. (2009) reported substantially lower  $S_n$  values, ranging from 0.51 to 0.64 for LWP between 107 and 143  $\text{g m}^{-2}$ , using MWRP-derived  $n_d$  and aerosol light scattering from a nephelometer.

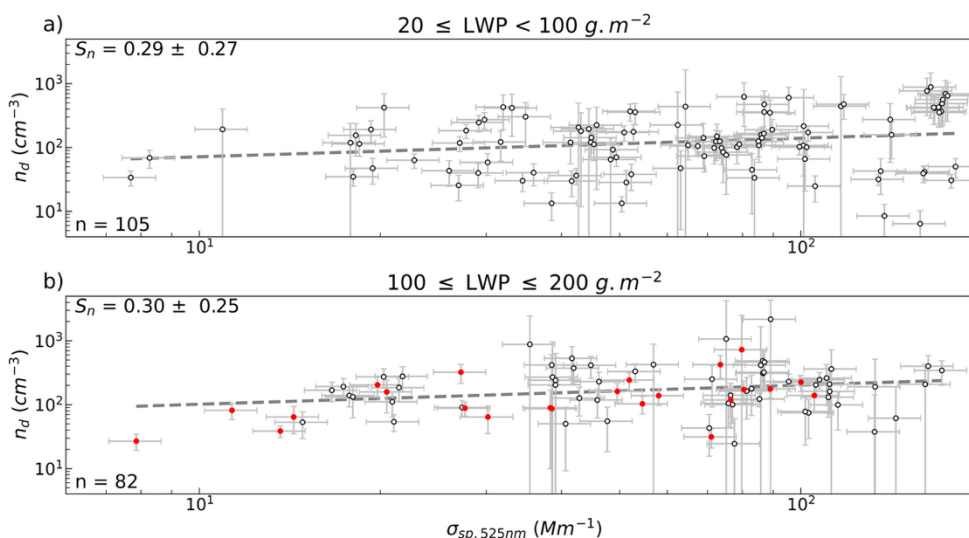


**Figure 4 : Retrievals of cloud droplet number concentration ( $n_d$ ) versus surface measurements of light scattering by dried haze aerosol  $\sigma_{sp,525nm}$  when the dataset is constrained for  $20 < \text{LWP} < 100 \text{ g m}^{-2}$  (a) and for  $100 < \text{LWP} < 200 \text{ g m}^{-2}$  (b). The red circles represent cases with  $\text{LWP} > 150 \text{ g m}^{-2}$ . The “nucleation efficiency”  $S_n$  is described by Equation 3 and the uncertainty is derived from the 95% confidence interval of the linear fit.  $n$  represents the numbers of data points used to draw each figure.**

## 4.2 Cloud droplet effective radius

As for the  $n_d$  analysis,  $r_e$  is plotted as a function of the aerosol scattering coefficient ( $\sigma_{sp,525nm}$ ) as shown in Figure 3, showing that  $r_e$  decreases as the scattering coefficient increases: considering the linear fit function, for a scattering coefficient of 8  $\text{Mm}^{-1}$ , the median  $r_e$  is 11.7  $\mu\text{m}$ , whereas for 180  $\text{Mm}^{-1}$  it is 9.0  $\mu\text{m}$  for low LWP. This trend indicates that increased aerosol scattering is associated with smaller cloud droplet sizes. For large LWP values, the median  $r_e$  is 11.5  $\mu\text{m}$  when the scattering coefficient is around 8  $\text{Mm}^{-1}$ , whereas for 171  $\text{Mm}^{-1}$  it is 9.1  $\mu\text{m}$ . The  $S_{r_e}$ , relating the droplet effective radius susceptibility to the aerosol burden, is defined as:

$$310 \quad S_{r_e} = \frac{-d\ln(r_e)}{d\ln(\sigma_{sp})} \quad (4)$$



Since  $r_e$  depends on LWP, Equation 4 should ideally be evaluated for a fixed LWP value as suggested by Feingold (2003). Over Lille, the  $S_{re}$  lies between the reported values with  $0.08 \pm 0.08$  and  $0.07 \pm 0.09$  for high and low LWP ranges, respectively. The uncertainties were assessed similarly to those for  $S_n$  using a 95% confidence interval. This observation is consistent with established research on  $S_{re}$ , which suggests that higher aerosol concentrations lead to a greater number of smaller droplets due to increased competition for available water vapor (McComiskey et al., 2009; Feingold et al., 2003).

Based on cloud-radar estimates of  $r_e$  and Raman-lidar aerosol extinction, Feingold (2003) derived  $S_{re}$  of 0.03–0.16 for a set of seven cases observed over the DOE ARM Southern Great Plains site in Oklahoma. Over the same site, Kim et al. (2008) found  $S_{re}$  values between 0.04 and 0.17 in continental stratus from a 3-year study. In the Arctic, Garrett et al. (2004) found  $S_{re}$  varying between 0.13 and 0.19 from similar instrumentation as was used here. Feingold et al. (2001) found  $S_{re}$  ranging from 0.12 to 0.38 using satellite retrievals of effective radius and nearby aerosol optical depth in smoke-affected conditions over Brazil. By contrast, Bréon et al. (2002) reported substantially smaller  $S_{re}$  over land, equal to 0.04, based on global satellite measurements of  $r_e$  and an aerosol index derived from submicrometer aerosol scattering coefficients.

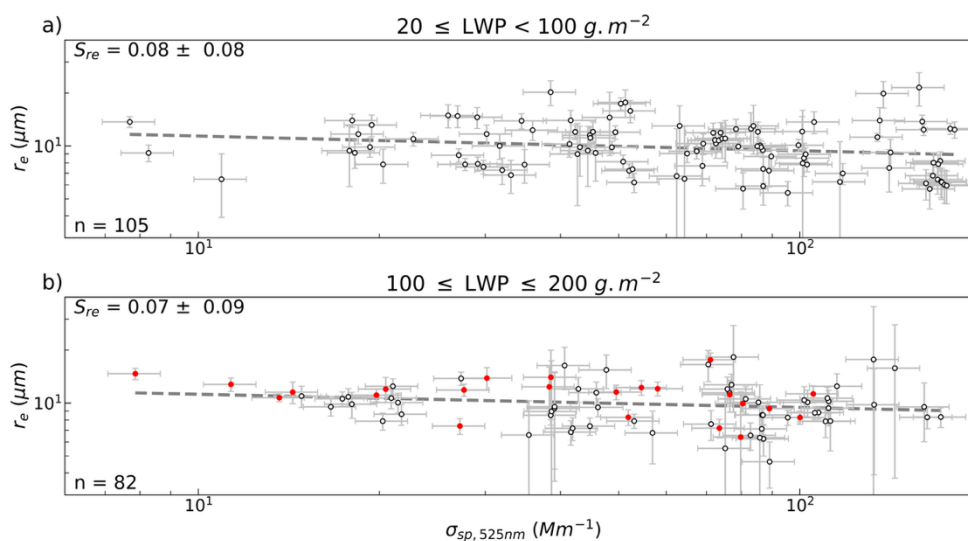


**Figure 5:** Retrievals of cloud effective radius ( $r_e$ ) versus surface measurements of light scattering by dried haze aerosol  $\sigma_{sp,525nm}$  when the dataset is constrained for  $20 < LWP < 100 \text{ g m}^{-2}$  (a) and for  $100 < LWP < 200 \text{ g m}^{-2}$ . The red circles represent cases with  $LWP > 150 \text{ g m}^{-2}$ . The aerosol cloud-droplet-size interaction parameter  $S_{re}$  is described by equation 4. The data are sorted according to the magnitude of cloud LWP.  $n$  represents the numbers of data points used to draw each figure.

For both  $n_d$  and  $r_e$ , the susceptibility uncertainties are somewhat larger than the susceptibility values themselves. Increasing the number of data points, by including additional ACTRIS sites, for example, may substantially reduce uncertainties or permit increasing the number of LWP bins. Zheng et al. (2020) were able to estimate cloud effective radius susceptibilities for 6 LWP



bins using ground-based measurements alone, and show that susceptibility tends to be largest for smaller LWP values. A similar tendency appears to be present here; however, the large uncertainties prevent this behaviour from being statistically confirmed.

## 330 5 Conclusions

Our results show a case study for how cloud droplet concentration and radius susceptibilities can be evaluated by combining ground-based measurements of aerosols with satellite retrievals of cloud microphysics. The methodology describes different criteria used to compare aerosol properties measured (aerosol scattering coefficient) at the ground with cloud properties ( $r_e$ ,  $n_d$ ) retrievals from satellite observations. From 5 years of data, cases were analysed where (1) the cloud base height is within the BL height, (2) the atmosphere is convectively stable, (3) there is only one cloud layer and finally (4) aerosols are large enough to act as CCN. For this subset, we observed that the  $r_e$  decreased and cloud droplet number concentration increased as aerosol loading increased. More interestingly, the cloud droplet concentration susceptibility to aerosol scattering coefficient ( $S_n$ ) was estimated at 0.29 and 0.30 for both LWP bins (above and below  $100 \text{ g m}^{-2}$ ) while the cloud droplet effective radius susceptibility to aerosol loading ( $S_{re}$ ) remained below 0.08 for both LWP bins. These findings underscore the critical role of aerosols in modulating cloud properties and, consequently, their impact on climate systems. However, the limited availability of data has restricted our ability to achieve statistically robust results and to apply additional criteria on aerosol chemical composition for example.

A limitation of our study is that satellite observations have coarser resolution than ground-based observations which affects the quantification of cloud susceptibilities to aerosol loading (McComiskey & Feingold, 2012). However, the baseline uncertainty associated with any individual approach remains high. For example, Jia et al. (2021) argued that studies based on satellite observations can underestimate the susceptibilities by 55% compared to studies based on ground-based stations. While this study is based on a single ACTRIS site in northern France (ATOLL), the methodology is readily extendable to other stations within the ACTRIS network. Many of these sites operate high-quality in-situ aerosol instrumentation and are increasingly collocated with remote sensing facilities capable of characterizing cloud properties. Sites such as SIRTA (Paris, France), Hyytiala (Finland) or Cabauw (Netherlands) span a variety of aerosol and meteorological regimes—from clean continental to polluted boundary layers. Expanding the methodology to a coordinated subset of ACTRIS stations would not only allow for a systematic assessment of regional contrasts in aerosol-cloud interactions, but also increase the statistical robustness of the observed relationships. Furthermore, the integration of collocated aerosol chemical composition measurements—mass spectrometry or filter-based analyses for example—would enable a more refined constraint on cloud microphysical responses and help disentangle the influence of aerosol hygroscopicity and mixing state (Zhang et al., 2015).



**Data availability :** ATOLL in-situ measurements are available through the EBAS database (<https://ebas.nilu.no>) and SMPS data before 2020 through <https://doi.org/10.5281/zenodo.6794562> (Crumeysrolle et al., 2022). The CLAAS-3 data set can be  
360 found online ([https://doi.org/10.5676/EUM\\_SAF\\_CM/CLAAS/V003](https://doi.org/10.5676/EUM_SAF_CM/CLAAS/V003)).

**Author contribution:** SC, QC and TG jointly designed the study. Data analysis and the construction of figures were made by SC and QC. EB ensure that all ATOLL instruments are working properly, SC reviewed the quality of in-situ data and OP the MWRP data. All authors were involved in drafting and reviewing the manuscript.  
365

**Competing interests:** Some authors are members of the editorial board of journal ACP.

**Acknowledgements:** This research was supported by the French national research agency (ANR) under the MABCaM (ANR-16-CE04-0009) contract. Part of the instrumental system has been financially supported by the CaPPA project (Chemical and  
370 Physical Properties of the Atmosphere), which is funded by the French National Research Agency (ANR) through the PIA (Programme d'Investissement d'Avenir) under contract “ANR-11-LABX-0005-01”, and by the Regional Council “Hauts-de-France”. ATOLL is a French component of the Aerosol, Clouds and Trace Gases Research Infrastructure (ACTRIS, <https://www.actris.eu/>). The French State under the France- 2030 program and the initiative of the Excellence of the University of Lille are acknowledged for the funding and support granted to the R-CDP-24-003-AREA project. The authors also thank  
375 the Région Hauts-de-France, the Ministère de l'Enseignement Supérieur et de la Recherche (CPER Climibio).

## 6 References

- Bellouin, N., Quaas, J., Gryspeerdt, E., Kinne, S., Stier, P., Watson-Parris, D., et al. (2020). Bounding global aerosol radiative forcing of climate change. *Reviews of Geophysics*, 58, e2019RG000660, 2020. <https://doi.org/10.1029/2019RG000660>
- 380 Benas, N., Solodovnik, I., Stengel, M., Hüser, I., Karlsson, K.-G., Håkansson, N., Johansson, E., Eliasson, S., Schröder, M., Hollmann, R., Meirink, J.F., 2023. CLAAS-3: the third edition of the CM SAF cloud data record based on SEVIRI observations. *Earth System Science Data* 15, 5153–5170. <https://doi.org/10.5194/essd-15-5153-2023>
- Bennartz, R. and Rausch, J.: Global and regional estimates of warm cloud droplet number concentration based on 13 years of AQUA-MODIS observations, *Atmos. Chem. Phys.*, 17, 9815–9836, <https://doi.org/10.5194/acp-17-9815-2017>, 2017.
- 385 Boichu, M., Favez, O., Riffault, V., Petit, J.-E., Zhang, Y., Brogniez, C., Sciare, J., Chiapello, I., Clarisse, L., Zhang, S., Pujol-Söhne, N., Tison, E., Delbarre, H., Goloub, P., 2019. Large-scale particulate air pollution and chemical fingerprint of volcanic sulfate aerosols from the 2014–2015 Holuhraun flood lava eruption of Bárðarbunga volcano (Iceland). *Atmospheric Chemistry and Physics* 19, 14253–14287. <https://doi.org/10.5194/acp-19-14253-2019>



- Boucher, O., Randall, D., Artaxo, P., et al. (2013). Clouds and Aerosols. In: *Climate Change 2013: The Physical Science Basis*.  
390 Cambridge University Press.
- Bovchaliuk, V., Goloub, P., Podvin, T., Veselovskii, I., Tanre, D., Chaikovskiy, A., Dubovik, O., Mortier, A., Lopatin, A.,  
Korenskiy, M., Victori, S., 2016. Comparison of aerosol properties retrieved using GARRLiC, LIRIC, and Raman algorithms  
applied to multi-wavelength lidar and sun/sky-photometer data. *Atmos. Meas. Tech.* 9, 3391–3405.  
<https://doi.org/10.5194/amt-9-3391-2016>
- 395 Breon, F.-M., D. Tanre, and S. Generoso, Aerosol effect on cloud droplet size monitored from satellite, *Science*, 295, 834–  
838, 2002.
- Chen, G., Canonaco, F., Tobler, A., Aas, W., Alastuey, A., Allan, J., Atabakhsh, S., Aurela, M., Baltensperger, U., Bougiatioti,  
A., De Brito, J.F., Ceburnis, D., Chazau, B., Chebaicheb, H., Daellenbach, K.R., Ehn, M., El Haddad, I., Eleftheriadis, K.,  
Favez, O., Flentje, H., Font, A., Fossun, K., Freney, E., Gini, M., Green, D.C., Heikkinen, L., Herrmann, H., Kalogridis, A.-  
400 C., Keernik, H., Lhotka, R., Lin, C., Lunder, C., Maasikmets, M., Manousakas, M.I., Marchand, N., Marin, C., Marmureanu,  
L., Mihalopoulos, N., Močnik, G., Nęcki, J., O’Dowd, C., Ovadnevaite, J., Peter, T., Petit, J.-E., Pikridas, M., Matthew Platt,  
S., Pokorná, P., Poulain, L., Priestman, M., Riffault, V., Rinaldi, M., Rózański, K., Schwarz, J., Sciare, J., Simon, L., Skiba,  
A., Slowik, J.G., Sosedova, Y., Stavroulas, I., Styszko, K., Teinmaa, E., Timonen, H., Tremper, A., Vasilescu, J., Via, M.,  
Vodička, P., Wiedensohler, A., Zografou, O., Cruz Minguillón, M., Prévôt, A.S.H., 2022. European Aerosol Phenomenology  
405 - 8: Harmonised Source Apportionment of Organic Aerosol using 22 Year-long ACSM/AMS Datasets. *Environment  
International* 107325. <https://doi.org/10.1016/j.envint.2022.107325>
- Cimini, C.; Marzano, F.S.; Ciotti, P.; Cimini, D.; Westwater, E.R.; Han, Y.; Keihm, S.J.; Ware, R. Atmospheric Microwave  
Radiative Models Study Based on Ground-Based Multichannel Radiometer Observations in the 20–60 GHz Band. In  
*Proceedings of the Fourteenth ARM Science Team Meeting Proceedings*, Albuquerque, NM, USA, 22–26 March 2004.
- 410 CMSAF: Algorithm Theoretical Basis Document, Cloud Physical Products, SEVIRI, EUMETSAT Satellite Application  
Facility on Climate Monitoring, SAF/CM/KNMI/ATBD/SEVIRI/PPP, Issue 3.2 [data set],  
[https://doi.org/10.5676/EUM\\_SAF\\_CM/CLAAS/V003](https://doi.org/10.5676/EUM_SAF_CM/CLAAS/V003), 20 May 2022b.
- Coopman, Q., Garrett, T. J., Finch, D. P., & Riedi, J. (2018). High sensitivity of arctic liquid clouds to long-range  
anthropogenic aerosol transport. *Geophysical Research Letters*, 45, 372–381. <https://doi.org/10.1002/2017GL075795>
- 415 Collaud Coen, M., Praz, C., Haeefe, A., Ruffieux, D., Kaufmann, P., Calpini, B., 2014. Determination and climatology of the  
planetary boundary layer height above the Swiss plateau by in situ and remote sensing measurements as well as by the  
COSMO-2 model. *Atmospheric Chemistry and Physics* 14, 13205–13221. <https://doi.org/10.5194/acp-14-13205-2014>
- Crumeyrolle, S., Kontkanen, J., Rose, C., Velasquez Garcia, A., Bourriane, E., Catalfamo, M., Riffault, V., Tison, E., Ferreira  
de Brito, J., Visez, N., Ferlay, N., Auriol, F., Chiapello, I., 2022. Measurement report: Atmospheric new particle formation in  
420 a peri-urban site in Lille, Northern France. *Atmospheric Chemistry and Physics Discussions* 1–35. [https://doi.org/10.5194/acp-  
2022-436](https://doi.org/10.5194/acp-2022-436)



- Crumeyrole, S., Kontkanen, J., Rose, C., Velasquez Garcia, A., Bourriane, E., Catalfamo, M., Riffault, V., Tison, E., Ferreira de Brito, J., Visez, N., Ferlay, N., Auriol, F., and Chiapello, I.: Measurement report: Atmospheric new particle formation in a peri-urban site in Lille, Northern France, *Atmospheric Chem. Phys. Discuss.*, 1–35, [data set],  
425 [https://zenodo.org/record/6794562#.Y5ITwi\\_pPuQ](https://zenodo.org/record/6794562#.Y5ITwi_pPuQ), 2022.
- Duran, B. M., Wall, C. J., Lutsko, N. J., Michibata, T., Ma, P.-L., Qin, Y., Duffy, M. L., Medeiros, B., and Debolskiy, M.: A new method for diagnosing effective radiative forcing from aerosol-cloud interactions in climate models, *Atmos. Chem. Phys.*, 25, 2123–2146, <https://doi.org/10.5194/acp-25-2123-2025>, 2025.
- Dusek, U., Frank, G. P., Hildebrandt, L., Curtius, J., Schneider, J., Walter, S., ... & Andreae, M. O. (2006). Size matters more than chemistry for cloud-nucleating ability of aerosol particles. *Science*, 312(5778), 1375-1378.  
430 <https://www.science.org/doi/10.1126/science.1125261>
- Fan, J., Y. Wang, D. Rosenfeld, and X. Liu, 2016: Review of Aerosol-Cloud Interactions: Mechanisms, Significance, and Challenges. *J. Atmos. Sci.*, 73, 4221–4252, <https://doi.org/10.1175/JAS-D-16-0037.1>.
- Feingold, G., L. A. Remer, J. Ramaprasad, and Y. Kaufman (2001), Analysis of smoke impact on clouds in Brazilian biomass  
435 burning regions: An extension of Twomey’s approach, *J. Geophys. Res.*, 106, 22,907 – 22,922, doi:10.1029/2001JD000732.
- Feingold, G., W. L. Eberhard, D. E. Veron, and M. Previdi (2003), First measurements of the Twomey indirect effect using ground-based remote sensors, *Geophys. Res. Lett.*, 30, 1287, doi:[10.1029/2002GL016633](https://doi.org/10.1029/2002GL016633), 6.
- Forster, P., T. Storelvmo, K. Armour, W. Collins, J.-L. Dufresne, D. Frame, D.J. Lunt, T. Mauritsen, M.D. Palmer, M. Watanabe, M. Wild, and H. Zhang, 2021: The Earth’s Energy Budget, Climate Feedbacks, and Climate Sensitivity. In *Climate Change 2021: The Physical Science Basis. Contribution of Working Group I to the Sixth Assessment Report of the Intergovernmental Panel on Climate Change* [Masson-Delmotte, V., P. Zhai, A. Pirani, S.L. Connors, C. Péan, S. Berger, N. Caud, Y. Chen, L. Goldfarb, M.I. Gomis, M. Huang, K. Leitzell, E. Lonnoy, J.B.R. Matthews, T.K. Maycock, T. Waterfield, O. Yelekçi, R. Yu, and B. Zhou (eds.)]. Cambridge University Press, Cambridge, United Kingdom and New York, NY, USA, pp. 923–1054, doi:10.1017/9781009157896.009.
- 445 Garrett, T.J., Zhao, C., Dong, X., Mace, G.G., Hobbs, P.V., 2004. Effects of varying aerosol regimes on low-level Arctic stratus. *Geophys. Res. Lett.* 31, L17105. <https://doi.org/10.1029/2004GL019928>
- Garrett, T.J., Zhao, C., 2013. Ground-based remote sensing of thin clouds in the Arctic. *Atmospheric Measurement Techniques* 6, 1227–1243. <https://doi.org/10.5194/amt-6-1227-2013>
- Grosvenor, D. P., et al. (2018). *Remote sensing of droplet number concentration in warm clouds: a review of the current state of knowledge and perspectives*. *Reviews of Geophysics*, 56, 409–453. <https://doi.org/10.1029/2017RG000593>
- 450 Gryspeerdt, E., Quaas, J., Bellouin, N., 2016. Constraining the aerosol influence on cloud fraction. *Journal of Geophysical Research: Atmospheres* 121, 3566–3583. <https://doi.org/10.1002/2015JD023744>
- Jia, H., Ma, X., Yu, F. *et al.* Significant underestimation of radiative forcing by aerosol–cloud interactions derived from satellite-based methods. *Nat Commun* 12, 3649 (2021). <https://doi.org/10.1038/s41467-021-23888-1>



- 455 Jokinen, V., Mäkelä, J.M., 1997. Closed-loop arrangement with critical orifice for DMA sheath/excess flow system. *Journal of Aerosol Science* 28, 643–648. [https://doi.org/10.1016/S0021-8502\(96\)00457-0](https://doi.org/10.1016/S0021-8502(96)00457-0)
- Karstens, U., Simmer, C., Ruprecht, E., 1994. Remote sensing of cloud liquid water. *Meteorol. Atmos. Phys.* 54, 157–171. <https://doi.org/10.1007/BF01030057>.
- Kim, G.-G., M. A. Miller, S. E. Schwartz, Y. Liu, and Q. Min (2008), The role of adiabaticity in the aerosol first  
460 indirect effect, *J. Geophys. Res.*, 113, D05210, doi:[10.1029/2007JD008961](https://doi.org/10.1029/2007JD008961)
- Kim, YJ., Kim, BG., Miller, M. *et al.* Enhanced aerosol-cloud relationships in more stable and adiabatic clouds. *Asia-Pacific J Atmos Sci* 48, 283–293 (2012). <https://doi.org/10.1007/s13143-012-0028-0>
- Klein, S.A., Hartmann, D.L., 1993. The Seasonal Cycle of Low Stratiform Clouds. *Journal of Climate* 6, 1587–1606. [https://doi.org/10.1175/1520-0442\(1993\)006%253C1587:TSCOLS%253E2.0.CO;2](https://doi.org/10.1175/1520-0442(1993)006%253C1587:TSCOLS%253E2.0.CO;2)
- 465 Laj, P., Bigi, A., Rose, C., Andrews, E., Lund Myhre, C., Collaud Coen, M., Lin, Y., Wiedensohler, A., Schulz, M., Ogren, J.A., Fiebig, M., Gliß, J., Mortier, A., Pandolfi, M., Petäjä, T., Kim, S.-W., Aas, W., Putaud, J.-P., Mayol-Bracero, O., Keywood, M., Labrador, L., Aalto, P., Ahlberg, E., Alados Arboledas, L., Alastuey, A., Andrade, M., Artíñano, B., Ausmeel, S., Arsov, T., Asmi, E., Backman, J., Baltensperger, U., Bastian, S., Bath, O., Beukes, J.P., Brem, B.T., Bukowiecki, N., Conil, S., Couret, C., Day, D., Dayantolis, W., Degorska, A., Eleftheriadis, K., Fetfatzis, P., Favez, O., Flentje, H., Gini, M.I.,  
470 Gregorič, A., Gysel-Ber, M., Hallar, A.G., Hand, J., Hoffer, A., Hueglin, C., Hooda, R.K., Hyvärinen, A., Kalapov, I., Kalivitis, N., Kasper-Giebl, A., Kim, J.E., Kouvarakis, G., Kranjc, I., Krejci, R., Kulmala, M., Labuschagne, C., Lee, H.-J., Lihavainen, H., Lin, N.-H., Löschau, G., Luoma, K., Marinoni, A., Martins Dos Santos, S., Meinhardt, F., Merkel, M., Metzger, J.-M., Mihalopoulos, N., Nguyen, N.A., Ondracek, J., Pérez, N., Perrone, M.R., Petit, J.-E., Picard, D., Pichon, J.-M., Pont, V., Prats, N., Prenni, A., Reisen, F., Romano, S., Sellegri, K., Sharma, S., Schauer, G., Sheridan, P., Sherman, J.P., Schütze,  
475 M., Schwerin, A., Sohmer, R., Sorribas, M., Steinbacher, M., Sun, J., Titos, G., Toczko, B., Tuch, T., Tulet, P., Tunved, P., Vakkari, V., Velarde, F., Velasquez, P., Villani, P., Vratolis, S., Wang, S.-H., Weinhold, K., Weller, R., Yela, M., Yus-Diez, J., Zdimal, V., Zieger, P., Zikova, N., 2020. A global analysis of climate-relevant aerosol properties retrieved from the network of Global Atmosphere Watch (GAW) near-surface observatories. *Atmos. Meas. Tech.* 13, 4353–4392. <https://doi.org/10.5194/amt-13-4353-2020>
- 480 Lihavainen, H., Kerminen, V.-M., and Remer, L. A.: Aerosol-cloud interaction determined by both in situ and satellite data over a northern high-latitude site, *Atmos. Chem. Phys.*, 10, 10987–10995, <https://doi.org/10.5194/acp-10-10987-2010>, 2010.
- Louf, V., Pujol, O., Sauvageot, H., Riédi, J., 2015. Seasonal and diurnal water vapour distribution in the Sahelian area from microwave radiometric profiling observations. *Quarterly Journal of the Royal Meteorological Society* 141, 2643–2653. <https://doi.org/10.1002/qj.2550>
- 485 Madhavan BL, He Y, Wu Y, Gross B, Moshary F, Ahmed S. Development of a Ground Based Remote Sensing Approach for Direct Evaluation of Aerosol-Cloud Interaction. *Atmosphere*. 2012; 3(4):468-494. <https://doi.org/10.3390/atmos3040468>



- Mascaut, F., Pujol, O., Verreyken, B., Peroni, R., Metzger, J.M., Blarel, L., Podvin, T., Goloub, P., Sellegri, K., Thornberry, T., Duflot, V., Tulet, P., Brioude, J., 2022. Aerosol characterization in an oceanic context around Reunion Island (AEROMARINE field campaign). *Atmospheric Environment* 268, 118770. <https://doi.org/10.1016/j.atmosenv.2021.118770>
- 490 Mascaut, F., Pujol, O., Brioude, J., Jensen, A., Lefranc, M., Evan, S., Crumeyrolle, S., 2023a. A competition–species model for water vapour-aerosol-cloud-rain interactions. *Atmospheric Research* 284, 106588. <https://doi.org/10.1016/j.atmosres.2022.106588>
- Mascaut, F., Pujol, O., Brioude, J., Jensen, A., 2023b. A 2D Ising-like model for cloud field organization in pristine oceans. *Eur. Phys. J. Plus* 138, 76. <https://doi.org/10.1140/epjp/s13360-022-03633-3>
- 495 MacDonald, A. B., Hossein Mardi, A., Dadashazar, H., Azadi Aghdam, M., Crosbie, E., Jonsson, H. H., ... & Sorooshian, A. (2020). On the relationship between cloud water composition and cloud droplet number concentration. *Atmospheric Chemistry and Physics*, 20(12), 7645-7665. <https://acp.copernicus.org/articles/20/7645/2020/>
- McComiskey, A. and Feingold, G.: The scale problem in quantifying aerosol indirect effects, *Atmos. Chem. Phys.*, 12, 1031–1049, <https://doi.org/10.5194/acp-12-1031-2012>, 2012.
- 500 McComiskey, A., G. Feingold, A. S. Frisch, D. D. Turner, M. A. Miller, J. C. Chiu, Q. Min, and J. A. Ogren (2009), An assessment of aerosol-cloud interactions in marine stratus clouds based on surface remote sensing, *J. Geophys. Res.*, 114, D09203, doi:[10.1029/2008JD011006](https://doi.org/10.1029/2008JD011006).
- Moreira, G. de A., Guerrero-Rascado, J.L., Bravo-Aranda, J.A., Foyo-Moreno, I., Cazorla, A., Alados, I., Lyamani, H., Landulfo, E., Alados-Arboledas, L., 2020. Study of the planetary boundary layer height in an urban environment using a combination of microwave radiometer and ceilometer. *Atmospheric Research* 240, 104932. <https://doi.org/10.1016/j.atmosres.2020.104932>
- Miri, R., Pujol, O., Hu, Q., Goloub, P., Veselovskii, I., Podvin, T., Ducos, F., 2024. Innovative aerosol hygroscopic growth study from Mie-Raman-fluorescence lidar and microwave radiometer synergy. *Atmospheric Measurement Techniques* 17, 3367–3375. <https://doi.org/10.5194/amt-17-3367-2024>
- 510 Michibata, T. (2022). Aerosol-Cloud Interactions in the Climate System. In: Akimoto, H., Tanimoto, H. (eds) *Handbook of Air Quality and Climate Change*. Springer, Singapore. [https://doi.org/10.1007/978-981-15-2527-8\\_35-1](https://doi.org/10.1007/978-981-15-2527-8_35-1)
- Mortier, A., Goloub, P., Podvin, T., Deroo, C., Chaikovsky, A., Ajtai, N., Blarel, L., Tanre, D., Derimian, Y., 2013. Detection and characterization of volcanic ash plumes over Lille during the Eyjafjallajökull eruption. *Atmos. Chem. Phys.* 13, 3705–3720. <https://doi.org/10.5194/acp-13-3705-2013>
- 515 Motos, G., Freitas, G., Georgakaki, P., Wieder, J., Li, G., Aas, W., ... & Nenes, A. (2023). Aerosol and dynamical contributions to cloud droplet formation in Arctic low-level clouds. *Atmospheric Chemistry and Physics*, 23(21), 13941-13956. <https://acp.copernicus.org/articles/23/13941/2023/>
- Müller, T., Laborde, M., Kassell, G., Wiedensohler, A., 2011. Design and performance of a three-wavelength LED-based total scatter and backscatter integrating nephelometer. *Atmos. Meas. Tech.* 4, 1291–1303. <https://doi.org/10.5194/amt-4-1291-2011>



- 520 Müller, T., Nowak, A., Wiedensohler, A., Sheridan, P., Laborde, M., Covert, D.S., Marinoni, A., Imre, K., Henzing, B., Roger, J.-C., Santos, S.M. dos, Wilhelm, R., Wang, Y.-Q., Leeuw, G. de, 2009. Angular Illumination and Truncation of Three Different Integrating Nephelometers: Implications for Empirical, Size-Based Corrections. *Aerosol Science and Technology* 43, 581–586. <https://doi.org/10.1080/02786820902798484>
- Nandan, R., Ratnam, M. V., Kiran, V. R., & Naik, D. N. (2022). Aerosol-cloud interaction in water clouds observed using  
525 ground-based, in-situ, and satellite-based observations over an Indian continental region. *Atmospheric Research*, 280, 106436.
- Nakajima, T. and King, M. D.: Determination of the optical thick-ness and effective particle radius of clouds from reflected solar radiation measurements, part 1: Theory, *J. Atmos. Sci.*, 47, 1878–1893, [https://doi.org/10.1175/1520-0469\(1990\)047<1878:DOTOTA>2.0.CO;2](https://doi.org/10.1175/1520-0469(1990)047<1878:DOTOTA>2.0.CO;2), 1990.
- Pandolfi, M., Alastuey, A., Reche, C., et al. (2021). ACTRIS: A European Aerosol, Clouds, and Trace Gases Research  
530 Infrastructure. *Atmospheric Environment*.
- Pavolonis, M. J., Heidinger, A. K., and Uttal, T.: Daytime global cloud typing from AVHRR and VIIRS: Algorithm description, validation, and comparison, *J. Appl. Meteorol.*, 44, 804–826, <https://doi.org/10.1175/JAM2236.1>, 2005.
- Petters, M. D., & Kreidenweis, S. M. (2007). A Single Parameter Representation of Hygroscopic Growth and Cloud Condensation Nucleus Activity. *Atmospheric Chemistry and Physics*.
- 535 Platnick, S., King, M. D., Ackerman, S. A., Menzel, W. P., Baum, B. A., Riédi, J. C., & Frey, R. A. (2003). The MODIS cloud products: Algorithms and examples from Terra. *IEEE Transactions on Geoscience and Remote Sensing*, 41(2), 459-473.
- Pruppacher, H.R., et J.D. Klett. « Microstructure of Atmospheric Clouds and Precipitation ». In *Microphysics of Clouds and Precipitation*, édité par H.R. Pruppacher et J.D. Klett. Springer Netherlands, 2010. [https://doi.org/10.1007/978-0-306-48100-0\\_2](https://doi.org/10.1007/978-0-306-48100-0_2).
- 540 Qiu, Y., Zhao, C., Guo, J., & Li, J. (2017). 8-Year ground-based observational analysis about the seasonal variation of the aerosol-cloud droplet effective radius relationship at SGP site. *Atmospheric Environment*, 164, 139-146.
- Quaas, J., et al. (2010). *Constraining the total aerosol indirect effect in the LMDZ and ECHAM4 GCMs using MODIS satellite data*. *Atmospheric Chemistry and Physics*, 10, 6137–6152. <https://doi.org/10.5194/acp-10-6137-2010>
- Quaas, J., Ming, Y., Menon, S., Takemura, T., Wang, M., Penner, J.E., Gattelman, A., Lohmann, U., Bellouin, N., Boucher, O., Sayer, A.M., Thomas, G.E., McComiskey, A., Feingold, G., Hoose, C., Kristjánsson, J.E., Liu, X., Balkanski, Y., Donner, L.J., Ginoux, P.A., Stier, P., Grandey, B., Feichter, J., Sednev, I., Bauer, S.E., Koch, D., Grainger, R.G., Kirkev&aring, G. A., Iversen, T., Seland, Ø., Easter, R., Ghan, S.J., Rasch, P.J., Morrison, H., Lamarque, J.-F., Iacono, M.J., Kinne, S., Schulz, M., 2009. Aerosol indirect effects – general circulation model intercomparison and evaluation with satellite data. *Atmospheric Chemistry and Physics* 9, 8697–8717. <https://doi.org/10.5194/acp-9-8697-2009>
- 550 Quaas, J., Arola, A., Cairns, B., Christensen, M., Deneke, H., Ekman, A.M.L., Feingold, G., Fridlind, A., Gryspeerdt, E., Hasekamp, O., Li, Z., Lipponen, A., Ma, P.-L., Mülmenstädt, J., Nenes, A., Penner, J.E., Rosenfeld, D., Schrödner, R., Sinclair, K., Sourdeval, O., Stier, P., Tesche, M., van Diedenhoven, B., Wendisch, M., 2020. Constraining the Twomey effect from



- satellite observations: issues and perspectives. *Atmospheric Chemistry and Physics* 20, 15079–15099. <https://doi.org/10.5194/acp-20-15079-2020>
- 555 Rose, C., Collaud Coen, M., Andrews, E., Lin, Y., Bossert, I., Lund Myhre, C., Tuch, T., Wiedensohler, A., Fiebig, M., Aalto, P., Alastuey, A., Alonso-Blanco, E., Andrade, M., Artíñano, B., Arsov, T., Baltensperger, U., Bastian, S., Bath, O., Beukes, J.P., Brem, B.T., Bukowiecki, N., Casquero-Vera, J.A., Conil, S., Eleftheriadis, K., Favez, O., Flentje, H., Gini, M.I., Gómez-Moreno, F.J., Gysel-Beer, M., Hallar, A.G., Kalapov, I., Kalivitis, N., Kasper-Giebl, A., Keywood, M., Kim, J.E., Kim, S.-W., Kristensson, A., Kulmala, M., Lihavainen, H., Lin, N.-H., Lyamani, H., Marinoni, A., Martins Dos Santos, S., Mayol-  
560 Bracero, O.L., Meinhardt, F., Merkel, M., Metzger, J.-M., Mihalopoulos, N., Ondracek, J., Pandolfi, M., Pérez, N., Petäjä, T., Petit, J.-E., Picard, D., Pichon, J.-M., Pont, V., Putaud, J.-P., Reisen, F., Sellegri, K., Sharma, S., Schauer, G., Sheridan, P., Sherman, J.P., Schwerin, A., Sohmer, R., Sorribas, M., Sun, J., Tulet, P., Vakkari, V., van Zyl, P.G., Velarde, F., Villani, P., Vratolis, S., Wagner, Z., Wang, S.-H., Weinhold, K., Weller, R., Yela, M., Zdimas, V., Laj, P., 2021. Seasonality of the particle number concentration and size distribution: a global analysis retrieved from the network of Global Atmosphere Watch (GAW)  
565 near-surface observatories. *Atmospheric Chemistry and Physics* 21, 17185–17223. <https://doi.org/10.5194/acp-21-17185-2021>
- Rosenfeld, D., Sherwood, S., Wood, R., Donner, L., 2014. Climate Effects of Aerosol-Cloud Interactions. *Science* 343, 379–380. <https://doi.org/10.1126/science.1247490>
- Sarna, K. and Russchenberg, H. W. J.: Ground-based remote sensing scheme for monitoring aerosol-cloud interactions, *Atmos. Meas. Tech.*, 9, 1039–1050, <https://doi.org/10.5194/amt-9-1039-2016>, 2016.
- Schmetz, J., Pili, P., Tjemkes, S., Just, D., Kerkmann, J., Rota, S., and Ratier, A.: An introduction to Meteosat second generation (MSG), *B. Am. Meteorol. Soc.*, 83, 977–992, <https://doi.org/10.1175/BAMS-83-7-Schmetz-2>, 2002.
- Sena, E. T., McComiskey, A., and Feingold, G.: A long-term study of aerosol-cloud interactions and their radiative effect at the Southern Great Plains using ground-based measurements, *Atmos. Chem. Phys.*, 16, 11301–11318,  
575 <https://doi.org/10.5194/acp-16-11301-2016>, 2016.
- Sinclair, Victoria Anne, Jenna Ritvanen, Gabin Urbancic, et al. « Boundary-Layer Height and Surface Stability at Hyytiälä, Finland, in ERA5 and Observations ». *Atmospheric Measurement Techniques* 15, n° 10 (2022): 3075-103. <https://doi.org/10.5194/amt-15-3075-2022>.
- Stephens, G.L., 1978. Radiation Profiles in Extended Water Clouds. I: Theory. *Journal of the Atmospheric Sciences* 35, 2111–  
580 2122. [https://doi.org/10.1175/1520-0469\(1978\)035%253C2111:RPIEWC%253E2.0.CO;2](https://doi.org/10.1175/1520-0469(1978)035%253C2111:RPIEWC%253E2.0.CO;2)
- Velazquez-Garcia, A., Crumeyrolle, S., de Brito, J.F., Tison, E., Bourriane, E., Chiapello, I., Riffault, V., 2023. Deriving composition-dependent aerosol absorption, scattering and extinction mass efficiencies from multi-annual high time resolution observations in Northern France. *Atmospheric Environment* 298, 119613. <https://doi.org/10.1016/j.atmosenv.2023.119613>



- 585 Villani, P., Picard, D., Marchand, N., Laj, P., 2007. Design and validation of a 6-volatility tandem differential mobility analyzer (VTDMA). *Aerosol Science and Technology* 41, 898–906. <https://doi.org/10.1080/02786820701534593>
- Watson-Parris, D., Smith, C.J. Large uncertainty in future warming due to aerosol forcing. *Nat. Clim. Chang.* 12, 1111–1113 (2022). <https://doi.org/10.1038/s41558-022-01516-0>
- Wolters, E. L. A., Roebeling, R. A., & Stammes, P. (2006). *Cloud reflectance calculations using DAK: study on required*  
590 *integration points*. Koninklijk Nederlands Meteorologisch Instituut. Available from <http://www.knmi.nl/publications>.
- Zhang, R., & Jimenez, J. L. (2015). *Impact of aerosol size and chemistry on cloud condensation nuclei formation: Implications for the Twomey effect*. *Atmospheric Environment*, 101, 12-19. <https://doi.org/10.1016/j.atmosenv.2014.11.023>
- Zheng, X., Xi, B., Dong, X., Logan, T., Wang, Y., and Wu, P.: Investigation of aerosol-cloud interactions under different absorptive aerosol regimes using Atmospheric Radiation Measurement (ARM) southern Great Plains (SGP) ground-based  
595 measurements, *Atmos. Chem. Phys.*, 20, 3483–3501, <https://doi.org/10.5194/acp-20-3483-2020>, 2020.